Visualizing the Stoichiometry of Industrial-Style Co-Mo-S Catalysts with Single-Atom Sensitivity**

*Yuanyuan Zhu, Quentin M. Ramasse, Michael Brorson, Poul G. Moses, Lars P. Hansen, Christian F. Kisielowski, and Stig Helveg**

Abstract: The functional properties of transition metal dichalcogenides (TMDs) may be promoted by the inclusion of other elements. Here, we studied the local stoichiometry of single cobalt promoter atoms in an industrial-style MoS_2-based hydrotreating catalyst. Aberration-corrected scanning transmission electron microscopy and electron energy loss spectroscopy show that the Co atoms occupy sites at the (-100) S edge terminations of the graphite-supported MoS_2 nanocrystals in the catalyst. Specifically, each Co atom has four neighboring S atoms that are arranged in a reconstructed geometry, which reflects an equilibrium state. The structure agrees with complementary studies of catalysts that were prepared under vastly different conditions and on other supports. In contrast, a small amount of residual Fe in the graphite is found to compete for the S edge sites, so that promotion by Co is strongly sensitive to the purity of the raw materials. The present single-atom-sensitive analytical method therefore offers a guide for advancing preparative methods for promoted TMD nanomaterials.

Transition-metal dichalcogenide (TMD) materials have unique physicochemical properties,[1,2] which may benefit from incorporating other elements into the TMD structure.[3,4] For instance, chemical promotion is significant in nanocrystalline MoS_2 that is used in refineries for the catalytic removal of environmentally harmful sulfur from crude oil fractions. For this hydrodesulfurization (HDS) process, the activity is significantly increased by the addition of transition metals such as cobalt (or nickel), and the promoted activity is attributed to the so-called "Co-Mo-S" phase.[3] Previously, using spectroscopic techniques, it was shown that the Co-Mo-S phase consists of Co atoms that are attached to the catalytically important edges of the MoS_2 nanocrystals.[3] Furthermore, an atomic structure for the Co-Mo-S phase was proposed based on complementary model studies using scanning tunneling microscopy (STM)[5,6] and density functional theory (DFT) calculations.[6,7] However, relating the model structure to industrial-style Co-Mo-S catalysts remains ambiguous because the incorporation of Co into MoS_2 nanocrystals is sensitive to the synthetic procedure,[3] and because element identification at the edges of the industrial-style Co-Mo-S catalysts has so far lacked single-atom sensitivity.[8,9]
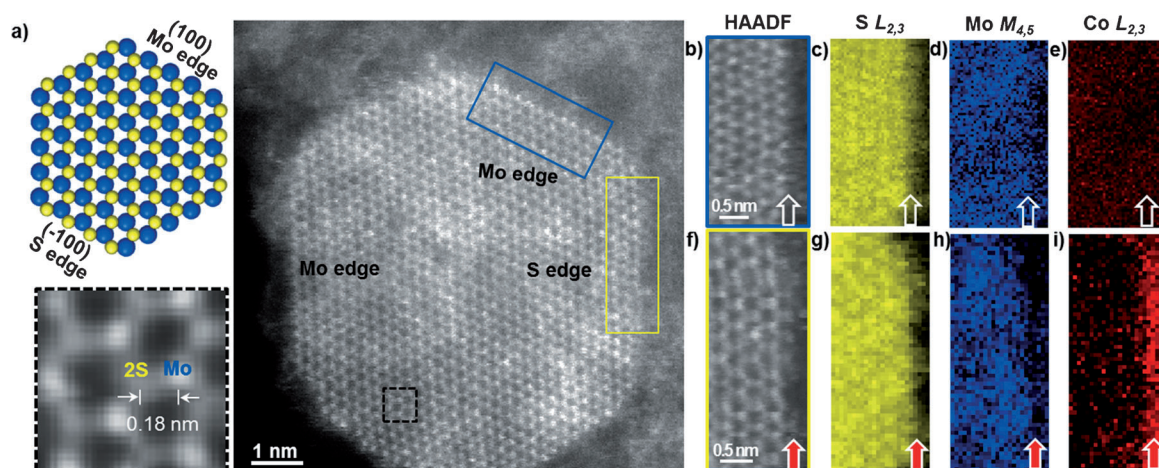
Recent advances in high-resolution (scanning) transmission electron microscopy ((S)TEM) imaging have opened up the possibility of studying two-dimensional materials with atomic-level resolution and sensitivity.[9–14] For instance, the elemental distribution in single- and double-layer MoS_2 nanocrystals was resolved with high-resolution TEM,[13] and high-angle annular dark-field (HAADF) STEM allowed for a distinction of the edge terminations.[14] Herein, we address the location of the Co promoter atoms in an industrial-style Co-Mo-S catalyst. A representative HAADF-STEM image of a hexagonally shaped Co-promoted MoS_2 nanocrystal that was supported on a graphite flake and oriented with its (001) basal plane along the graphite (001) plane and orthogonal to the electron beam direction is shown in Figure 1a. In the HAADF mode, the images are dominated by the Z-contrast, which ascribes a bright contrast to atomic column positions, and which, to a good approximation, scales with the square of the total projected atomic number of the columns. As in previous work,[14] the Z-contrast images of the MoS_2 basal plane present an asymmetric dumbbell structure reflecting a pair of atomic columns separated by 0.18 nm in the $<001>$ projection. This asymmetric dumbbell corresponds to the 1 Mo and 2 S columns, indicating the presence of single-layer MoS_2 nanocrystals and facilitating the assignment of the Mo edge and S edge terminations (Figure 1a).[14] Although image contrast quantification may in principle be applied to identify all types of atoms, in practice, the analysis usually suffers from uncertainties that arise from a non-uniform support contrast and the limited signal-to-noise (S/N) ratio for non-invasive observations with electron beams.[11,14] Therefore, to unambiguously determine the chemical arrangement in industrial-style Co-Mo-S nanocrystals, the present study combines HAADF-STEM with simultaneous electron energy loss (EEL) spectroscopy.[15]

[*] Y. Zhu, M. Brorson, P. G. Moses, L. P. Hansen, S. Helveg
Haldor Topsøe A/S
Nymøllevej 55, 2800 Kgs. Lyngby (Denmark)
E-mail: sth@topsoe.dk

Q. M. Ramasse
SuperSTEM Laboratory, STFC Daresbury
Keckwick Lane, Daresbury WA4 4AD (UK)

C. F. Kisielowski
Joint Center for Artificial Photosynthesis
National Center for Electron Microscopy
Lawrence Berkeley National Laboratory
1 Cyclotron Road, Berkeley, CA 94708 (USA)

Figure 1. a) Unprocessed HAADF-STEM image of a single-layer Co-Mo-S nanocrystal on a graphite support with the MoS$_2$ (001) plane orientated orthogonally to the electron beam direction (left). A ball model and an enlarged section of the interior lattice (right), showing the asymmetric 2S–1Mo dumbbell Z-contrast pattern, resolve the (100) Mo edge and (−100) S edge terminations as marked. Simultaneously recorded HAADF-STEM image and elemental maps are derived from the S $L_{2,3}$, Mo $M_{4,5}$, and Co $L_{2,3}$ ionization edges at the Mo edge (b–e) and S edge (f–i). Note that the S maps are atomically resolved with maxima at the S sublattice of the basal plane, whereas the Mo maps only provide a reference for the Mo distribution. Arrows mark the termination of the basal MoS$_2$ plane (open) and the position of Co atoms (red). The Co map also shows faint maxima suggesting near-atomic resolution.

First, for the MoS$_2$ nanocrystal that is shown in Figure 1a, a spectrum image, which consists of EEL spectra recorded serially pixel-by-pixel across a selected edge region, was used to determine the elemental content from the relative intensities of the S $L_{2,3}$, Mo $M_{4,5}$, and Co $L_{2,3}$ ionization edges (Supporting Information, Figure S1). Figure 1b–i shows the resulting elemental maps for the (100) Mo edge and (−100) S edge terminations of the MoS$_2$ nanocrystal. The maps reveal that the basal plane consists of Mo and S, and that S and Mo are the only constituent elements of the Mo edge.[14] The spectrum image also contains a C K signal (not reported) that is due to the graphite support. Here, the main finding is that the elemental maps unambiguously show a clear Co signal, which is confined to the sole S edge, and which has an appreciable intensity at the outer atomic row. This preference for Co to occupy positions at the S edge was confirmed for six additional single-layer MoS$_2$ nanocrystals (e.g., Figure S5). Interestingly, the Co maps show that the promoter atoms tend to fully cover the S edge, even in the presence of defects (Figure S6b).

Next, the precise atomic structure and stoichiometry at the S edge of the single-layer Co-Mo-S nanocrystal were determined by comparing the elemental maps with the HAADF-STEM image. Figure 2 shows an analysis for the S edge shown in Figure 1. The 2S and 1Mo column arrangement of the basal plane lattice is readily inferred from the HAADF contrast (Figure 2a). The 2S columns coincide with maxima in the S map (Figure 2c). However, because of the inelastic scattering process[16] and low S/N ratios, the Mo maps shown here are not atomically resolved. Nevertheless, Figure 2b,d shows that the Co signal mainly peaks at the Z-contrast maxima next to the 2S columns at the basal plane edge, and that the Z-contrast maxima appear slightly fainter than the Mo columns: These maxima are therefore attributed to Co. Thus, by combining the atomic positions indicated by
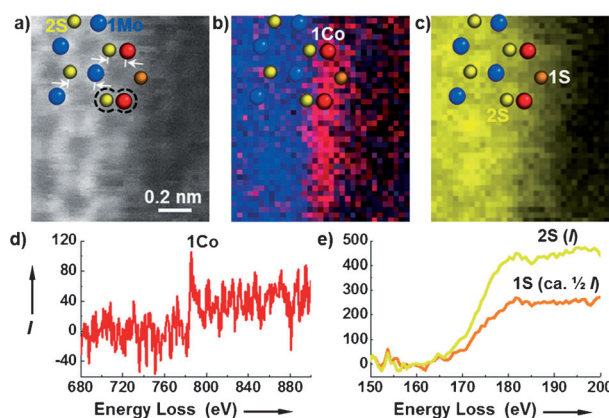
Figure 2. a) High-resolution HAADF-STEM image of the S edge in Figure 1a and corresponding b) Mo and Co and c) S maps. The ball model denotes the positions of the 1Mo (blue), 2S (yellow), 1Co (red), and 1S (orange) atom columns (Figure S2). d) Integrated Co $L_{2,3}$ ionization edge, representing the sum of six different 1Co atomic columns along the S edge. e) The $L_{2,3}$ edges of one 2S and one 1S atomic column in (c). Each atomic-column EEL spectrum was integrated over a window with a 3×3 pixel area (corresponding to the probe size in (a)).

the Z-contrast and the element type identified by EEL spectroscopy, it could be unambiguously shown that the Co atoms are occupying positions similar to the Mo sites as an extension of the MoS$_2$ basal plane, and that Co forms 2S–1Co dumbbells, as viewed in the MoS$_2$ <001> projection. Inspection of the Z-contrast line profiles also revealed that the 2S–1Co separation of approximately 0.16 nm (Co−S bond length ca. 0.22 nm) is shorter than the 2S–1Mo separation of 0.18 nm (Mo−S bond length: 0.24 nm; Figure S2). The EEL spectra show that Mo and Co are absent at positions further

away from the edge, but S was still detected. The S signal (albeit not as well defined as in the bulk of the nanocrystal because of lower S/N ratios) peaks at very faint Z-contrast maxima bridging the Co atoms at the very edge of the nanocrystal (Figure 2a). These maxima have just half of the S intensity of the 2S columns on the basal plane (Figure 2e) and are correspondingly assigned to single S atoms. Z-contrast line profiles show that the 1Co–1S separation is 0.19–0.22 nm, which is again consistent with a contraction of the Co−S bond compared to the Mo−S bond. Therefore, the 2S–1Co dumbbells at the S edge are terminated by a row of single S atoms so that the Co atoms are tetrahedrally coordinated to S atoms.

It should be noted that the acquisition of the present data at single-atom sensitivity required low electron doses because the catalyst is highly susceptible to electron beam damage. Such effects appeared as the removal of atoms (mainly at edges or corners) between successive images (Figure S5 and S6). To address the impact of the electron beam, HAADF-STEM images were therefore recorded before and after the acquisition of the spectroscopic data. Only spectroscopic results without noticeable lattice damage in those images were included in the present analysis (Figure S4).

Figure 3 summarizes the analysis in an atomistic picture: The industrial-style carbon-supported Co-Mo-S catalyst contains single Co atoms that are preferentially located at the
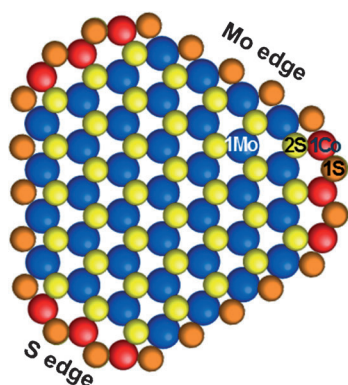

Figure 3. Top-view ball model of the industrial-style Co-Mo-S nanocrystal. The balls denote the position of the 1Mo (blue), 1Co (red), 2S (yellow), and 1S (orange) columns.

S edge of MoS_2 nanocrystals and tetrahedrally coordinated to S atoms. The structure of the unpromoted Mo edge termination of the MoS_2 nanocrystal was addressed previously (Figure S3).[14] The preferred location of Co in the present industrial-style Co-Mo-S nanocrystals is in agreement with previous STM[5,6] and DFT[6,7] studies. These studies considered Co-Mo-S nanocrystals that were formed on a Au(111) surface by a physical vapor deposition method under ultra-high vacuum conditions, or present in an unsupported state, respectively. Moreover, the observed contraction of the Co−S bond and the tetrahedral S coordination of Co are in agreement with X-ray absorption spectroscopic analysis for industrial-style alumina- and carbon-supported Co-Mo-S catalysts.[17] A comparison of the different model and industrial-

style Co-Mo-S catalysts shows similar structural characteristics, despite remarkable differences in their preparation, support, and sulfidation. In fact, the observation of the 1S reconstruction at the Co-promoted S edge and at the unpromoted Mo edge is in agreement with DFT calculations for unsupported Co-Mo-S particles.[7b,14,18] This agreement indicates that the present sulfidation conditions are adequate to equilibrate edge structures and that the Co-Mo-S/graphite interaction is sufficiently weak to leave that equilibrium structure unperturbed.

However, some of the inspected MoS_2 nanocrystals deviated from the Co-Mo-S structure. Figure 4a shows a single-layer MoS_2 nanocrystal for which the EEL spectra
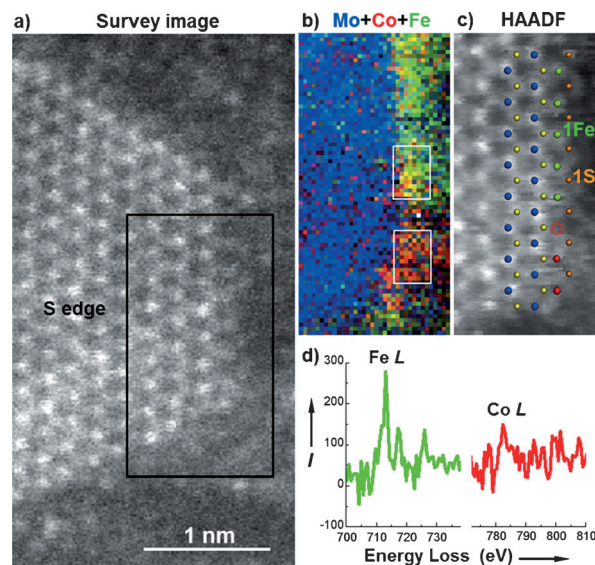
Figure 4. a) HAADF-STEM image of a MoS_2 nanocrystal. An EEL spectrum image was acquired over the S edge area framed in black. b) The corresponding combined Mo/Co/Fe map. The Fe and Co signals were integrated over a 40 eV window above their respective edge onsets. c) HAADF image at the S edge (framed in (a)) with a superimposed ball model indicating 1Co (red), 1Fe (green), 1Co (blue), 2S (yellow), and 1S (orange) column positions. d) Separate EEL spectra integrated over the white-framed regions in (b) showing the Fe and Co $L_{2,3}$ ionization edges. A slight structural change of a Co atom removal during EEL acquisition (marked by an open circle) does not affect the conclusion (Figure S4c).

unambiguously revealed a Co $L_{2,3}$ edge as well as an additional Fe $L_{2,3}$ edge (Figure 4b–d). An atom-by-atom analysis shows that Co and Fe atoms occupy similar sites (Figure 4c). This similarity is in agreement with previous model studies[19] and may be due to the fact that Co and Fe are neighboring transition metals, whereas W or Au substitutes into basal plane sites and lattice defects,[4,20] respectively. However, Fe was not intentionally added during the present synthesis. Therefore, the observed Fe species (Figure 4b) probably stem from Fe residues that were detected in the graphite support (see the Experimental Section).

In summary, the present analysis of an industrial-style carbon-supported Co-Mo-S catalyst reveals that single Co

promoter atoms are located preferentially at the S edges of MOS$_2$ nanocrystals with a tetrahedral coordination to S atoms. As a result, the Co promoter atoms become intrinsically undercoordinated to S atoms, an arrangement that has previously been proposed to be attractive for the adsorption of S-containing reactants.[5,6,7b] Moreover, the direct characterization of the Co-Mo-S structure agrees well with complementary studies of model and industrial-style catalysts. This independence of the synthesis route and the support materials suggests that the Co-Mo-S structure represents an equilibrated phase. The observations therefore make us optimistic that further interplay with model studies will uncover the role of the Co promoter atoms in industrial HDS catalysis. However, the fact that Fe residues compete with Co for S edge sites suggests that Co-Mo-S preparation is highly sensitive to the purity of the raw materials. As Fe does not promote HDS activity,[3,20] its presence lowers the fraction of the promoted Co-Mo-S sites. This finding may explain why carbon-supported Co-Mo-S catalysts tend to vary in activity depending on the type of carbon support.[3] Thus, the present analytical capability of pinpointing local atomic stoichiometry should be highly beneficial for developing preparative routes towards promoted MoS$_2$ catalysts and other nanomaterials with tunable functionalities.

Experimental Section

The industrial-style Co-promoted MoS$_2$ hydrotreating catalyst was prepared on a graphitic support by a sequential incipient wetness impregnation method.[21] First, a graphitic powder (Grade AO-2, Graphene Supermarket) was rinsed with oxalic acid to reduce the amount of metallic impurities, resulting in a residual Fe content of about 210 ppm. Second, the rinsed powder was tabletized and granulated. The graphite granulates were 1) impregnated with a Co(acetate)$_2$ solution (0.1 wt% Co), 2) dried under ambient conditions at 110°C, 3) dipped into an (NH$_4$)$_2$[MoS$_4$] solution (Mo loading ca. 0.3 wt%), and 4) dried. The nominal atomic ratio of Mo/Co was 3:1. Finally, the impregnated graphite was sulfided in 10% H$_2$S in H$_2$ at 1073 K for 6 hours, subsequently cooled in the sulfiding gas, and kept at room temperature in inert N$_2$. The samples were stored in a dry and oxygen-free nitrogen atmosphere, which was also used for TEM sample preparation.[13,14] Specifically, granulates were crushed in a mortar and dispersed dry on standard Cu TEM grids covered with lacey carbon.

Electron microscopy was carried out at the SuperSTEM Laboratory, Daresbury, using a Nion UltraSTEM100 dedicated aberration-corrected scanning transmission electron microscope. The microscope has an ultra-high vacuum below 5×10^{-9} Torr near the sample. The instrument is equipped with a cold-field emission gun with a native energy spread of 0.35 eV and was operated with a beam energy of 60 keV. The probe-forming optics were configured to provide a beam convergence semi-angle of 30 mrad, corresponding to a probe size of approximately 0.11 nm. An estimated electron beam current of about 50 pA was impinging on the sample. STEM images were acquired in HAADF mode with the detector inner and outer radii being calibrated at 85 mrad and 190 mrad, respectively. EEL spectra were recorded using a Gatan Enfina spectrometer, with a collection semi-angle of 37 mrad. An energy dispersion of 0.7 eV/channel was chosen so that the S $L_{2,3}$, Mo $M_{4,5}$, and Co $L_{2,3}$ ionization edges could all be recorded simultaneously. The dwell time was set to 50 ms/spectrum, which provided the best achievable compromise between acquisition speed and S/N ratio.[22] The data in Figures 1, 2, and 4 are simultaneously recorded HAADF-STEM and EEL spectrum

images. During analysis, all spectra were first processed using principal component analysis.[23] Subsequently, the electron energy dispersion was carefully calibrated using the S $L_{2,3}$ and Fe $L_{2,3}$ ionization edge onsets as internal references, whereas the C K edge onset was used to check for energy shifts. For generating elemental maps, the spectra were background-subtracted by fitting a power law model to electron energies lower than the edge onsets, and then intensity integration was done above the edge onset of the S $L_{2,3}$, Mo $M_{4,5}$ and Co $L_{2,3}$ signals, over windows of 20 eV, 40 eV, and 60 eV unless otherwise specified, at each spatial pixel. For generating the element map, no further smoothing or filtering of the EEL spectra was employed. HAADF-STEM images were reported as raw data, unless otherwise specified.

[1] a) R. Tenne, *Angew. Chem.* **2003**, *115*, 5280–5289; *Angew. Chem. Int. Ed.* **2003**, *42*, 5124–5132; b) Q. H. Wang, K. Kalantar-Zadeh, A. Kis, J. N. Coleman, M. S. Strano, *Nat. Nanotechnol.* **2012**, *7*, 699–712; c) M. Chhowalla, H. S. Shin, G. Eda, L. J. Li, K. P. Loh, H. Zhang, *Nat. Chem.* **2013**, *5*, 263–275.

[2] a) F. Besenbacher, M. Brorson, B. S. Clausen, S. Helveg, B. Hinnemann, J. Kibsgaard, J. V. Lauritsen, P. G. Moses, J. K. Nørskov, H. Topsøe, *Catal. Today* **2008**, *130*, 86–96; b) T. F. Jaramillo, K. P. Jørgensen, J. Bonde, J. H. Nielsen, S. Horch, I. Chorkendorff, *Science* **2007**, *317*, 100–102.

[3] H. Topsøe, B. S. Clausen, F. E. Massoth, *Hydrotreating Catalysis*, Springer, Berlin/Heidelberg, **1996**.

[4] Y. F. Chen, J. Y. Xi, D. O. Dumcenco, Z. Liu, K. Suenaga, D. Wang, Z. G. Shuai, Y. S. Huang, L. M. Xie, *ACS Nano* **2013**, *7*, 4610–4616.

[5] J. V. Lauritsen, S. Helveg, E. Lægsgaard, I. Stensgaard, B. S. Clausen, H. Topsøe, F. Besenbacher, *J. Catal.* **2001**, *197*, 1–5.

[6] J. V. Lauritsen, J. Kibsgaard, G. H. Olesen, P. G. Moses, B. Hinnemann, S. Helveg, J. K. Nørskov, B. S. Clausen, H. Topsøe, E. Lægsgaard, F. Besenbacher, *J. Catal.* **2007**, *249*, 220–233.

[7] a) L. S. Byskov, J. K. Nørskov, B. S. Clausen, H. Topsøe, *J. Catal.* **1999**, *187*, 109–122; b) H. Schweiger, P. Raybaud, H. Toulhoat, *J. Catal.* **2002**, *212*, 33–38.

[8] O. Sørensen, B. S. Clausen, R. Candia, H. Topsøe, *Appl. Catal.* **1985**, *13*, 363–372.

[9] F. L. Deepak, R. Esparza, B. Borges, X. Lopez-Lozano, M. Jose-Yacaman, *ACS Catal.* **2011**, *1*, 537–543.

[10] C. O. Girit, J. C. Meyer, R. Erni, M. D. Rossell, C. Kisielowski, L. Yang, C.-H. Park, M. F. Crommie, M. L. Cohen, S. G. Louie, A. Zettl, *Science* **2009**, *323*, 1705–1708.

[11] O. L. Krivanek, M. F. Chisholm, V. Nicolosi, T. J. Pennycook, G. J. Corbin, N. Dellby, M. F. Murfitt, C. S. Own, Z. S. Szilagyi, M. P. Oxley, S. T. Pantelides, S. J. Pennycook, *Nature* **2010**, *464*, 571–574.

[12] K. Suenaga, M. Koshino, *Nature* **2010**, *468*, 1088–1090.

[13] C. Kisielowski, Q. M. Ramasse, L. P. Hansen, M. Brorson, A. Carlsson, A. M. Molenbroek, H. Topsøe, S. Helveg, *Angew. Chem.* **2010**, *122*, 2768–2770; *Angew. Chem. Int. Ed.* **2010**, *49*, 2708–2710.

[14] L. P. Hansen, Q. M. Ramasse, C. Kisielowski, M. Brorson, E. Johnson, H. Topsøe, S. Helveg, *Angew. Chem.* **2011**, *123*, 10172–10172; *Angew. Chem. Int. Ed.* **2011**, *50*, 9994–9994.

[15] P. E. Batson, *Nature* **1993**, *366*, 727–728.

[16] L. J. Allen, S. D. Findlay, M. P. Oxley, *Scanning Transmission Electron Microscopy* (Eds.: S. J. Pennycook, P. D. Nellist), Springer, New York, **2011**, pp. 247–290.

[17] a) B. S. Clausen, B. Lengeler, R. Candia, J. Als-Nielsen, H. Topsøe, *Bull. Soc. Chim. Belg.* **1981**, *90*, 1249–1259; b) S. M. A. M. Bouwens, J. A. R. van Veen, D. C. Koningsberger, V. H. J. de Beer, R. Prins, *J. Phys. Chem.* **1991**, *95*, 123.

[18] P. G. Moses, B. Hinnemann, H. Topsøe, J. K. Nørskov, *J. Catal.* **2009**, *268*, 201–208.

[19] J. Kibsgaard, A. Tuxen, K. G. Knudsen, M. Brorson, H. Topsøe, E. Lægsgaard, J. V. Lauritsen, F. Besenbacher, *J. Catal.* **2010**, *272*, 195–203.

[20] Y. C. Lin, D. O. Dumcenco, H.-P. Komsa, Y. Niimi, A. V. Krasheninnikov, Y.-S. Huang, K. Suenaga, *Adv. Mater.* **2014**, *26*, 2857–2861.

[21] M. Brorson, A. Carlsson, H. Topsøe, *Catal. Today* **2007**, *123*, 31–36.

[22] R. Zan, Q. M. Ramasse, R. Jalil, T. Georgiou, U. Bangert, K. S. Novoselov, *ACS Nano* **2013**, *7*, 10167–10174.

[23] N. Bonnet, N. Brun, C. Colliex, *Ultramicroscopy* **1999**, *77*, 97–112.